

Title: Curved fault slip captured by CCTV video during the 2025 Mw 7.7
Mandalay earthquake.

Authors: Jesse Kearse¹ and Yoshihiro Kaneko¹

¹Graduate School of Science, Kyoto University, Japan.

Abstract

On-fault geological observations from surface breaking earthquakes typically contain curved slickenlines, suggesting fault slip is curved. However, slickenlines commonly record only a fraction of coseismic slip, making it difficult to reconstruct the full slip trajectory. Near-fault seismic records, though capable of capturing ground motions associated with rupture, are limited in their ability to constrain on-fault slip direction as they record motion on only one side of the fault. Here, we overcome these challenges by directly observing fault slip using video footage of the 2025 Mw 7.7 Mandalay (Myanmar) strike-slip earthquake. We use pixel cross correlation to track features in successive frames of the video, revealing a pulse of fault slip with a magnitude of 2.5 ± 0.5 m, duration of 1.3 ± 0.2 s, and peak velocity of 3.2 ± 1.0 m/s. The observed trajectory is notably curved, and includes a transient (0.3 m) dip slip component on a steeply dipping strike-slip fault. These observations are consistent with geological records of curved slickenlines supporting mechanical models that link rupture propagation direction to near-surface slip curvature. Our results provide the first direct visual evidence of curved coseismic fault slip, bridging a critical gap among seismological observations, geological data, and theoretical models.

Introduction

Resolving the dynamics of fault slip during large earthquake ruptures is a major challenge in earthquake science. On-fault geological data represent a valuable archive of slip in surface breaking earthquakes, recorded as slickenlines embedded into the fault plane itself (Spudich et al., 1998; Kearsse et al., 2019; Barth et al., 2024). Slickenlines are typically curved (Kearsse and Kaneko, 2020), suggesting fault motions evolve dynamically during seismic slip. However, inferring the full coseismic slip trajectory from slickenlines is challenging, as they typically record only a fraction of slip, or may form a complex network of overlapping striations (Kearsse and Kaneko, 2020). Because these observations are typically made days after the event, there is inherent uncertainty about the influence of non-seismic sources of slickenline formation, such as postseismic slip, or gravity-driven movement within the unstable ground surface rupture zone, limiting their potential to capture the dynamics of seismic slip.

Another approach to resolving the rate and direction of slip during earthquake rupture involves using near-field instrumental records—such as strong-motion seismometers or high-rate GNSS—since ground motions within a few kilometers of the fault are dominated by the direct effects of fault slip (the so-called near-field terms) (Bouchon et al., 2000; Kearsse et al., 2024). However, due to their off-fault location, it is unclear to what extent these records are contaminated by free surface effects, and whether they are able to resolve the cohesive zone of the propagating rupture (Cruz-Atienza et al., 2009). Furthermore, because instruments are typically located on only one side of the fault, reconstructing the relative motion between both sides is not straightforward.

In this paper, we overcome these challenges using CCTV video footage of ground surface rupture during the 2025 moment magnitude (Mw) 7.7 Mandalay earthquake (Myanmar), which provides the first direct observation of surface fault slip in real time. We track objects by pixel cross correlation in successive frames of the video to measure the rate and direction

of fault motion during coseismic slip. Our observations show that slip near the ground surface is distinctly curved. We demonstrate that these new observations are consistent with previous reports of curved slickenlines and recent models of dynamic rupture propagation, and discuss how these data provide an important link between physics-based earthquake simulations, on-fault geological data, and near-fault observations of strong ground motion.

Video analysis of the Mandalay earthquake

The Mw 7.7 2025 Mandalay earthquake occurred on March 28, with a hypocenter 20 km west of Mandalay city, Myanmar at a depth 10 km (USGS, 2025). The hypocenter location and right-lateral strike-slip mechanism are consistent with rupture on the Sagaing Fault, a major north-striking structure accommodating right-lateral shear between the Burma Plate to the west and Sundaland to the east (Vigny et al., 2003). The earthquake lasted approximately 90 seconds (Inoue et al., 2025), and propagated both north and south with total rupture length exceeding 400 km and surface strike slip exceeding 6 m (Fig. 1). Due to the exceptionally long rupture, strong ground shaking of Modified Mercalli Intensity (MMI) X extended over a broad area causing widespread damage to homes, sites of historical and cultural significance, and to key infrastructure in Myanmar, resulting in 3600 confirmed fatalities (Witze, 2025).

At the time of the earthquake, a CCTV security camera was recording video at the trace of the Sagaing Fault, 120 km south of earthquake hypocenter (Fig. 1). The camera was positioned approximately 20 m to the east of the Sagaing Fault, and was facing southwest across the Fault (Figs. 1b and 1c). The remarkable footage clearly shows relative northward translation of the western side of the fault during coseismic slip on the Sagaing Fault, which lasted approximately 2 seconds, and was accompanied by the simultaneous formation of a 1-2 meter wide moletrack along the surface rupture trace.

We use a windowed pixel cross correlation approach to measure the accrual of slip across

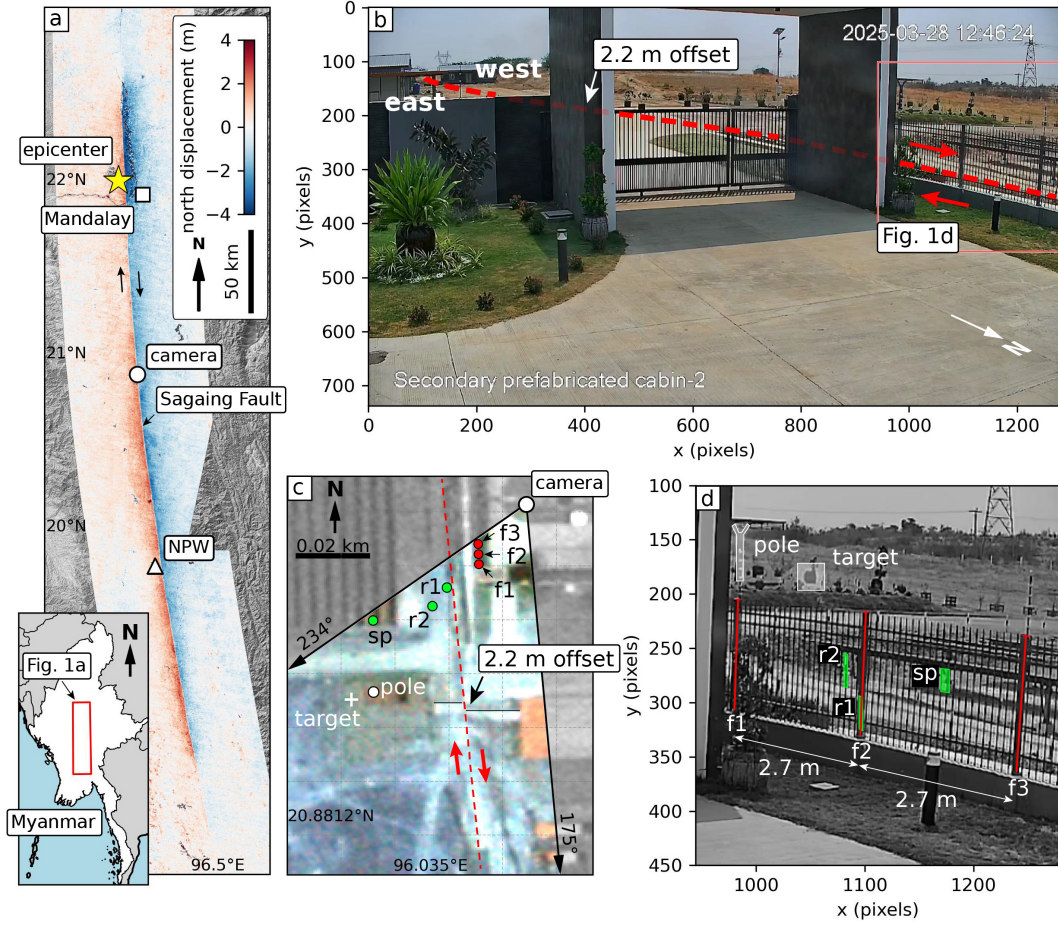


Figure 1: (a) Map of Myanmar (inset) and the Mandalay earthquake. Red and blue colors show the coseismic surface displacement field derived from sentinel-2 images taken before and after the earthquake from Van Wyk De Vries (2025). Location of CCTV camera and strong motion station NPW are shown. (b) Frame 1 of video (before rupture arrives) showing the field of view captured by the CCTV camera. Dashed red line shows the location of the Sagaing Fault rupture. Offset path is obscured behind the gate structure in the foreground. (c) Planet labs satellite image with a 0.5 m resolution taken after the earthquake (2025-04-05). Features observable in (d) are labeled. Colorized area corresponds to the field of view of the video frames in (b). f1-f3 denote fence posts located on the east side of the fault and used to calibrate coseismic displacements. r1, r2, sp, and pole, are objects that are displaced by fault motion. White cross labeled "target" shows the location of features tracked using image cross correlation. (d) Enlarged subset of the video frame showing the locations of the objects in pixel coordinates.

the Sagaing Fault from the first frame of the video (Fig. 2a) to the last frame (Fig. 2b). To track displacements on the west side of the fault, we define 25 overlapping 26x26-pixel windows each containing objects located 70 – 80 m from the camera. Our analysis is based primarily on the window that produced the sharpest cross correlation results ("target", Fig. 2a), however, our results are consistent across all windows. We also track features on the eastern side of the fault, the same side as the camera (e.g., "noise", Fig. 2a).

Figure 2c shows the displacement timeseries of tracked features relative to the image frame over the duration of the video. Ground shaking commences at 9.5 ± 0.1 s characterized by coherent motion of both features, and is followed by stronger shaking at 12 ± 0.1 s. The displacement timeseries of the target begins to diverge from the noise at 14.1 ± 0.1 s approximately 5 s after the first arrivals. Later at 15.4 ± 0.1 s both features resume their coherent, time-synchronized displacements, which continues until the last frame of the record. During this 1.3-second interval, the largest pixel displacements are observed for the target: +33 pixels in the positive x-direction and -13 pixels in the negative y-direction. In contrast, the feature on the near side of the fault shows relatively minor displacements: -1 pixel in x and -7 pixels in y.

To estimate the timeseries of slip across the Sagaing Fault, we follow a workflow to convert from pixel displacement to meters on the Sagaing Fault plane (Fig. S1, available in the electronic supplement to this article). First, we subtract the displacement timeseries of the noise from the target (Fig. 2c). This removes noise introduced by wobbling and tilting of the camera during ground shaking. Next, we use fence posts of known spacing and orientation (while accounting for lens distortion and parallax) to estimate displacements in units of meters at the target location (Figs. S3 and S4). By projecting the displacements along the fault parallel direction estimated from post-earthquake satellite imagery, we obtain the strike-slip and dip-slip components of relative fault motion (Fig. S6). To obtain the slip velocity function, we differentiate the displacement timeseries and apply a 0.2 s moving

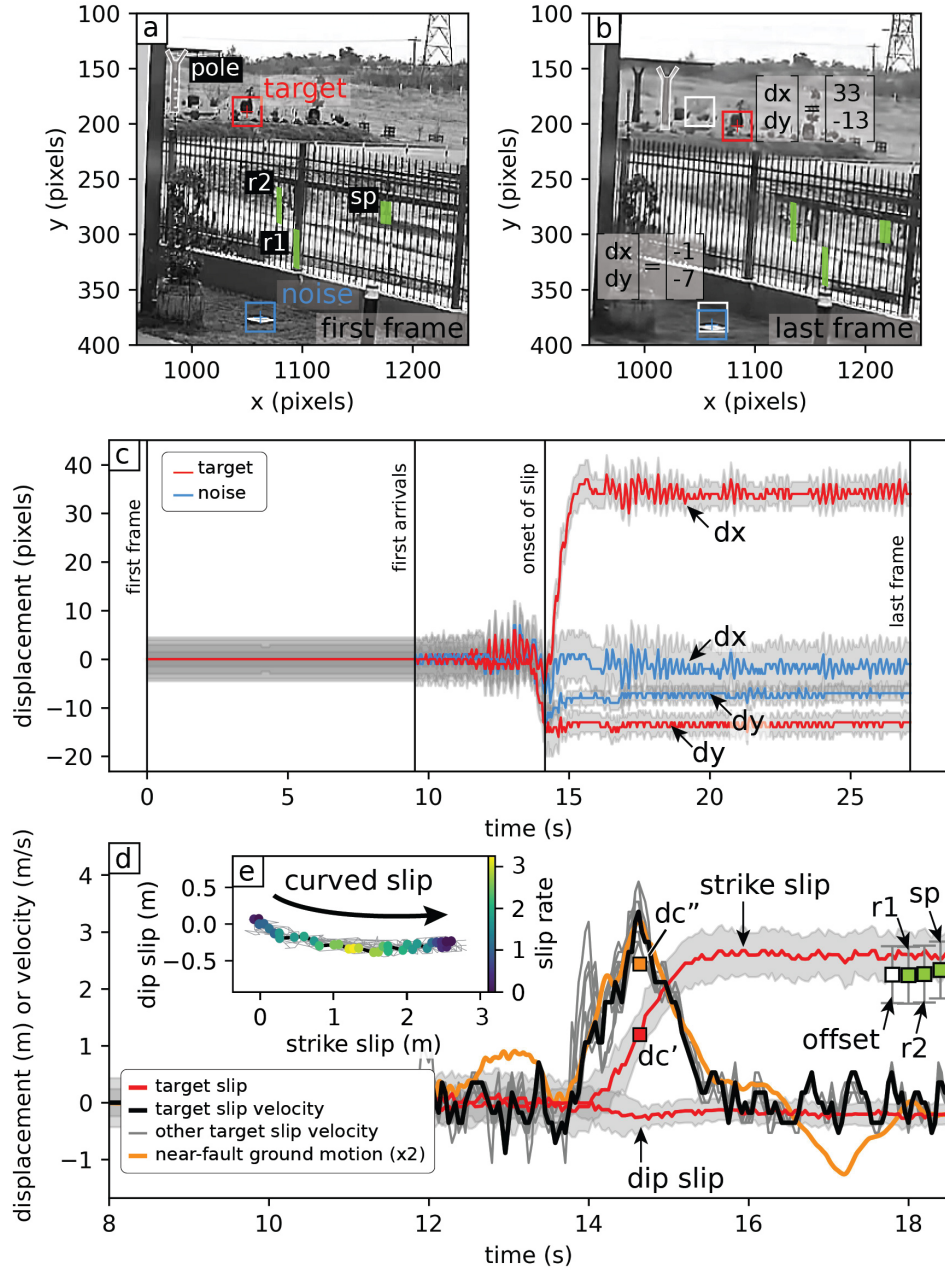


Figure 2: First frame (a) and last frame (b) of the CCTV video. Red box labeled "target" shows the 26-pixel window used to track displacements on the west (far) side of the Sagaing Fault, and on the east (near) side of the fault to correct for camera motion (blue box labeled "noise"). White boxes show the original pixel location of the target and noise in the first frame of the CCTV video. Location of roadside posts (r1, r2) and solar panel (sp) are shown. (c) Timeseries of pixel displacements as measured by pixel cross correlation or target (red) and noise (blue), y displacements are inverted such that positive y displacement represents positive vertical movement within the image. (d) Timeseries of fault slip (red) and slip velocity (black). Grey velocity curves show the results of additional targets for comparison. Fault parallel offset of the footpath is shown for comparison, as well as total slip measured for r1, r2, and sp (green squares). Amplitude of fault-parallel ground velocity at NPW (orange) is doubled to compare with slip velocity. Slip weakening distance derived from on-fault slip velocity (dc') and off-fault ground velocity (dc''). (e) Curved fault slip trajectory colored by slip velocity. Curvature occurs at the beginning of slip before slip reaches maximum velocity and slip < dc'.

average to suppress artifacts introduced by the discrete digital sampling (24 fps).

Coseismic slip of the Sagaing Fault

Our analysis reveals coseismic slip across the Sagaing Fault as a smooth ramp-like slip function with an amplitude of 2.5 ± 0.5 m and duration of 1.3 ± 0.2 s (Fig. 2d). Down-to-the-west dip-slip displacement reaches a maximum of 0.3 ± 0.25 m only 0.5 s after the onset of slip, and subsequently reducing to 0.2 ± 0.25 m. The magnitude of net slip agrees well with the post-earthquake satellite observation of a discrete footpath offset of 2.2 ± 0.5 m (e.g., Fig. 1c). We calculated additional displacements of 2.2 m, 2.2 m, 2.3 m for three objects located on the western side of the Sagaing Fault at distances of 5, 10, and 35 m from the fault trace, respectively (r1, r2, sp, Fig. 2d). The slight increase in fault-parallel displacement amplitude (from 2.2 to 2.5 m) with distance from the fault (0 - 35 m) aligns with previous field observations of on- and off-fault coseismic strain associated with other large strike-slip ruptures (Rockwell et al., 2002; Kearse et al., 2018).

Slip on Sagaing Fault reaches a peak rate of 3.2 ± 1 m/s at 14.6 ± 0.1 s, exhibiting a slightly asymmetric slip velocity envelope characterized by a longer deceleration tail (0.8 s) relative to the initial acceleration phase (0.5 s). For comparison, slip velocities derived from tracking additional targets are also shown (gray velocity curves, Fig. 2d), and exhibit similarly shaped velocity envelopes. The coseismic slip trajectory of the Sagaing Fault is dominated by right-lateral strike slip, and contains a non-zero time-dependent component of vertical slip resulting in slip curvature (Fig. 2e). The first meter of slip accumulation is oblique, containing a component of down-to-the-west motion across the fault. This corresponds to the initial 0.5 s of the rupture as slip velocity is increasing. The subsequent 1.5 m of slip is characterized by nearly pure strike-slip, corresponding to the final 0.8 s of rupture as slip velocity decreases and fault slip is arrested.

Our analysis demonstrates that the net slip direction is approximately horizontal, consis-

tent with strike-slip motion. However, due to the inherent non-uniqueness in transforming pixel displacements into real-world coordinates, the exact orientation of the net slip vector cannot be precisely resolved. Despite this limitation, the consistent curvature observed across multiple slip trajectories suggests that this feature is robust and independent of the precise slip direction.

Discussion and Conclusions

This video record provides the first direct observations of seismic fault slip in a natural earthquake. The observed slip duration (rise time of 1.3 s) and high slip velocity (>3 m/s) offer clear evidence of pulse-like rupture propagation at the site. While pulse-like rupture is commonly observed in large earthquakes (e.g., Melgar and Hayes, 2017), the mechanisms responsible for slip arrest remain debated. Proposed explanations include self-healing of slip governed by velocity-dependent friction (Heaton, 1990), or stopping phases generated either at fault strength barriers (Beroza and Mikumo, 1996), fault edges (Day, 1982), or within the fault damage zone (Huang and Ampuero, 2011). Stopping phases originating from the base of the fault are anticipated for elongated strike-slip ruptures that saturate the seismogenic width—conditions that are clearly met by the 2025 rupture of the Sagaing Fault. Modeling of rupture dynamics may provide some insight on this, but is beyond the scope of this paper.

Previously, on-fault evidence for time-varying slip direction has come primarily from curved slickenlines observed on exhumed fault planes. While suggestive of dynamic processes, such geological observations lack a direct temporal context, limiting their ability to resolve rupture dynamics. This study presents the first direct observation of curved fault slip, providing real-time validation that curved slickenlines can form during seismic rupture (Fig. 3). The geometry of the curved slip trajectory on the Sagaing Fault is consistent with curved slickenlines observed in other large strike-slip ruptures, such as the 2016 Mw 7.8 Kaikoura

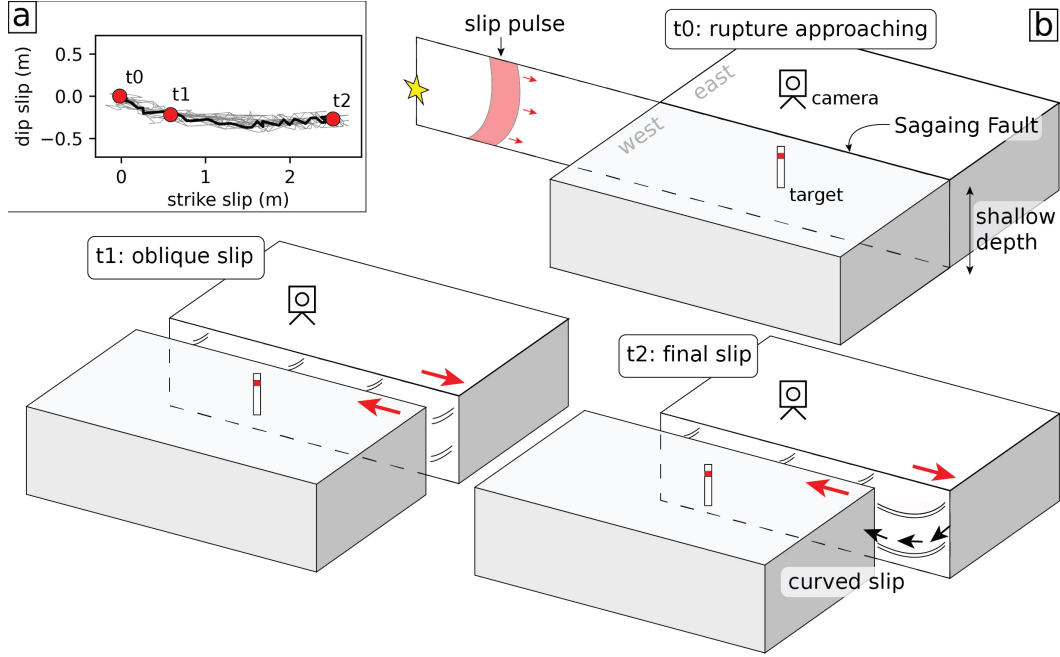


Figure 3: Cartoon illustrating coseismic slip evolution on the Sagaing Fault during the 2025 Mandalay earthquake. (a) Slip path of the Sagaing Fault during the earthquake showing three key time intervals corresponding to snapshots shown in (b). (b) Schematic snapshots of slip evolution as the rupture front approaches the CCTV observation site from the north: at initial seismic wave arrival (t_0), during early slip acceleration with an oblique trajectory including a down-to-the-west component (t_1), and after slip arrest (t_2). Black curves on the fault plane depict the slip path that would be recorded by slickenlines.

146 earthquake, New Zealand (Kearse et al., 2019). During rupture of the Kekerengu Fault in
147 2016, slip was initially oblique and subsequently curved to become dominantly strike-slip,
148 forming a curved slip trajectory that closely resembles that of the Sagaing Fault in 2025.

149 A key result of our analysis is the observation that slip on the Sagaing Fault curves rapidly
150 during the acceleration phase, but remains linear as slip decelerates (Fig. 2e), a relationship
151 that was not resolvable using geological data alone. This type of dynamic behavior during
152 slip onset is a feature observed across a suite of dynamic rupture simulations (Kaneko et al.,
153 2008; Kearse and Kaneko, 2020). These models suggest a mechanism for slip curvature
154 that is controlled by the dynamic stresses within the cohesive zone of the rupture, which is
155 dependent on the direction of rupture propagation. The curvature of slip on the Sagaing Fault
156 as the 2025 Mandalay earthquake rupture propagated southward past the CCTV camera is
157 consistent with these models, which predict transient uplift of the side of the fault moving
158 in the direction of rupture propagation (east side of the Sagaing Fault moves south and up),
159 relative to the other side of the fault.

160 Fault-parallel velocity pulses in near-fault strong-motion records have been used to esti-
161 mate the slip-weakening distance (d_c) on the nearby fault plane during rupture (Fukuyama
162 and Mikumo, 2007; Kaneko et al., 2017; Kearse et al., 2024). However, this approach lacks
163 direct on-fault observations of slip velocity, which are needed to validate the methods, and
164 to quantify the influence of off-fault free surface effects. This study provides the first op-
165 portunity to compare on-fault slip velocity and off-fault ground velocity at a strong-motion
166 station during the same earthquake rupture, and to compare estimates of slip-weakening
167 distances between the two. The strong motion station NPW (Lai et al., 2025) is located 2.7
168 km from the Sagaing Fault and 130 km further south along strike from the location of this
169 study (i.e. the rupture first arrived at the CCTV camera, and later at NPW). Figure 2d
170 displays the un-filtered fault-parallel component of ground velocity at NPW, but with its
171 amplitude doubled to allow a more direct comparison with the on-fault slip velocity function.

Both records show remarkable agreement, with similar amplitude, duration, and shape of the velocity function. This suggests that ground motions recorded at NPW likely reflect the off-fault signature of a pulse of slip on the nearby Sagaing Fault during the 2025 Mandalay earthquake. This comparison supports the use of near-fault ground velocity records to constrain key rupture parameters—such as local rise time and peak slip velocity—to first order. These quantities are often difficult to uniquely resolve with conventional kinematic inversion techniques (Guatteri and Spudich, 2000; Konca Ozgun et al., 2013). Slip-weakening distance estimated using the method of Fukuyama and Mikumo (2007) with the strong-motion data ($dc'' = 2.4$ m) is notably larger than that inferred from on-fault observations ($dc' = 1.2$ m). This discrepancy likely reflects the added complexity in the ground velocity time series at NPW, including challenges in isolating direct fault-slip phases from secondary free-surface effects (e.g., Yao and Yang, 2025).

Overall, these observations establish a new benchmark for understanding dynamic rupture processes. They offer real-time confirmation that curved slickenlines can form during seismic slip, reinforce model-based interpretations of slip curvature governed by rupture dynamics, and validate near-fault ground motion records as reliable proxies for on-fault slip behavior. Together, these findings impose critical observational constraints on future rupture simulations and deepen our understanding of the physical mechanisms that control rapid fault slip during large earthquakes.

References

- Barth, N. C., J. R. Kearse, T. A. Little, and R. J. Van Dissen, 2024: Rupture direction of paleoearthquakes on the Alpine Fault, New Zealand, as recorded by curved slickenlines. *Geology*, **52** (12), 917–921.
- Beroza, G. C., and T. Mikumo, 1996: Short slip duration in dynamic rupture in the pres-

ence of heterogeneous fault properties. *Journal of Geophysical Research: Solid Earth*,
101 (B10), 22 449–22 460.

Bouchon, M., N. Toksöz, H. Karabulut, M.-P. Bouin, M. Dietrich, M. Aktar, and M. Edie,
2000: Seismic imaging of the 1999 Izmit (Turkey) rupture inferred from the near-fault
recordings. *Geophysical Research Letters*, **27 (18)**, 3013–3016.

Cruz-Atienza, V. M., K. B. Olsen, and L. A. Dalguer, 2009: Estimation of the breakdown
slip from strong-motion seismograms: Insights from numerical experiments. *Bulletin of
the Seismological Society of America*, **99 (6)**, 3454–3469.

Day, S. M., 1982: Three-dimensional finite difference simulation of fault dynamics: rectan-
gular faults with fixed rupture velocity. *Bulletin of the Seismological Society of America*,
72 (3), 705–727.

Fukuyama, E., and T. Mikumo, 2007: Slip-weakening distance estimated at near-fault sta-
tions. *Geophysical Research Letters*, **34 (9)**.

Guatteri, M., and P. Spudich, 2000: What can strong-motion data tell us about slip-
weakening fault-friction laws? *Bulletin of the Seismological Society of America*, **90 (1)**,
98–116.

Heaton, T. H., 1990: Evidence for and implications of self-healing pulses of slip in earthquake
rupture. *Physics of the Earth and Planetary Interiors*, **64 (1)**, 1–20.

Huang, Y., and J.-P. Ampuero, 2011: Pulse-like ruptures induced by low-velocity fault zones.
Journal of Geophysical Research: Solid Earth, **116 (B12)**.

Inoue, N., R. Yamaguchi, Y. Yagi, R. Okuwaki, E. Bogdan, and T. Tadapansawut, 2025: A
multiple asymmetric bilateral rupture sequence derived from the peculiar tele-seismic P-

waves of the 2025 Mandalay, Myanmar earthquake. *Seismica*, **4** (1), doi:10.26443/seismica.v4i1.1691, URL <https://seismica.library.mcgill.ca/article/view/1691>.

Kaneko, Y., E. Fukuyama, and I. J. Hamling, 2017: Slip-weakening distance and energy budget inferred from near-fault ground deformation during the 2016 Mw7. 8 Kaikōura earthquake. *Geophysical Research Letters*, **44** (10), 4765–4773.

Kaneko, Y., N. Lapusta, and J.-P. Ampuero, 2008: Spectral element modeling of spontaneous earthquake rupture on rate and state faults: Effect of velocity-strengthening friction at shallow depths. *Journal of Geophysical Research: Solid Earth*, **113** (B9).

Kearse, J., and Y. Kaneko, 2020: On-fault geological fingerprint of earthquake rupture direction. *Journal of Geophysical Research: Solid Earth*, **125** (9), e2020JB019863.

Kearse, J., Y. Kaneko, T. Little, and R. Van Dissen, 2019: Curved slickenlines preserve direction of rupture propagation. *Geology*, **47** (9), 838–842.

Kearse, J., Y. Kaneko, Y. Nozuka, C. Milliner, Y. J. Hsu, and J.-P. Avouac, 2024: Strong asymmetry in near-fault ground velocity during an oblique strike-slip earthquake revealed by waveform particle motions and dynamic rupture simulations. *Seismica*, **3** (2), 1–12.

Kearse, J., and Coauthors, 2018: Onshore to offshore ground-surface and seabed rupture of the Jordan–Kekerengu–Needles fault network during the 2016 Mw 7.8 Kaikōura earthquake, New Zealand. *Bulletin of the Seismological Society of America*, **108** (3B), 1573–1595.

Konca Ozgun, A., Y. Kaneko, N. Lapusta, and J.-P. Avouac, 2013: Kinematic inversion of physically plausible earthquake source models obtained from dynamic rupture simulations. *Bulletin of the Seismological Society of America*, **103** (5), 2621–2644.

- Lai, S.-T., and Coauthors, 2025: Capacity Building Enables Unique Near-Fault Observations of the destructive 2025 M_w 7.7 Myanmar Earthquake. *Earth System Science Data Discussions*, **2025**, 1–23.
- Melgar, D., and G. P. Hayes, 2017: Systematic observations of the slip pulse properties of large earthquake ruptures. *Geophysical Research Letters*, **44** (19), 9691–9698.
- Rockwell, T. K., S. Lindvall, T. Dawson, R. Langridge, W. Lettis, and Y. Klinger, 2002: Lateral offsets on surveyed cultural features resulting from the 1999 Izmit and Duzce earthquakes, Turkey. *Bulletin of the Seismological Society of America*, **92** (1), 79–94.
- Spudich, P., M. Guatteri, K. Otsuki, and J. Minagawa, 1998: Use of fault striations and dislocation models to infer tectonic shear stress during the 1995 Hyogo-ken Nanbu (Kobe) earthquake. *Bulletin of the Seismological Society of America*, **88** (2), 413–427.
- USGS, 2025: M 7.7 - 2025 Mandalay, Burma (Myanmar) Earthquake. <https://earthquake.usgs.gov/earthquakes/eventpage/us7000pn9s/executive>.
- Van Wyk De Vries, M., 2025: 2025 Myanmar earthquake displacement maps. Zenodo, doi: 10.5281/zenodo.15123647.
- Vigny, C., A. Socquet, C. Rangin, N. Chamot-Rooke, M. Pubellier, M.-N. Bouin, G. Bertrand, and M. Becker, 2003: Present-day crustal deformation around Sagaing fault, Myanmar. *Journal of Geophysical Research: Solid Earth*, **108** (B11).
- Witze, A., 2025: Deadly Myanmar earthquake was probably a rare rupture, scientists say. *Nature*, **640** (8058), 296–297.
- Yao, S., and H. Yang, 2025: Rupture phases reveal geometry-related rupture propagation in a natural earthquake. *Science Advances*, **11** (4), eadq0154.